Effects of Melittin on Molecular Dynamics and Ca-ATPase Activity in Sarcoplasmic Reticulum Membranes: Time-Resolved Optical Anisotropy†

John Voss, Woubalem Birmachu, Deborah M. Hussey, and David D. Thomas*
Department of Biochemistry, University of Minnesota Medical School, Minneapolis, Minnesota 55455
Received February 12, 1991; Revised Manuscript Received May 6, 1991

ABSTRACT: We have studied the effect of melittin, a basic membrane-binding peptide, on Ca-ATPase activity and on protein and lipid dynamics in skeletal sarcoplasmic reticulum (SR), using time-resolved phosphorescence and fluorescence spectroscopy. Melittin completely inhibits Ca-ATPase activity, with half-maximal inhibition at 9 ± 1 mol of melittin bound to the membrane per mole of ATPase (0.1 mol of melittin per mole of lipid). The time-resolved phosphorescence anisotropy (TPA) decay of the Ca-ATPase labeled with erythrosin isothiocyanate (ERITC) shows that melittin restricts microsecond protein rotational motion. At 25 °C in the absence of melittin, the TPA is characterized by three decay components, corresponding to a rapid segmental motion (correlation time ϕ_1 = 2–3 μs), the uniaxial rotation of monomers or dimers (ϕ_2 = 16–22 μs), and the uniaxial rotation of larger oligomers (ϕ_3 = 90–140 μs). The effect of melittin is primarily to decrease the fraction of the more mobile monomer/dimer species (A_2) while increasing the fractions of the larger oligomer (A_3) and very large aggregates (A_∞). Time-resolved fluorescence anisotropy of the lipid-soluble probe diphenylhexatriene (DPH) shows only a slight increase in the lipid hydrocarbon chain effective order parameter, corresponding to an increase in lipid viscosity that is too small to account for the large decrease in protein mobility or inhibition of Ca-ATPase activity. Thus the inhibitory effect of melittin correlates with its capacity to aggregate the Ca-ATPase and is consistent with previously reported inhibition of this enzyme under conditions that increase protein–protein interactions. The ionic strength dependence of melittin's effects were investigated and compared with those of polylysine. These results suggest that the ability of melittin to both inhibit and immobilize the Ca-ATPase cannot be accounted for by electrostatic interactions alone, as can those of polylysine, but that a substantial component of melittin's effect on the enzyme can be attributed to hydrophobic interactions of melittin with the membrane.

Protein–protein interactions have been proposed to play an important role in the function of the Ca-ATPase in sarcoplasmic reticulum (SR). A fundamental problem that has yet to be solved is that of the quaternary structure of the Ca-ATPase. Various physical methods have been used to investigate the quaternary structure of the enzyme. The results have been conflicting, suggesting that the enzyme may exist as a monomer, dimer, or higher order oligomer. Time-resolved phoshorescence anisotropy (TPA) measurements of Ca-ATPase show a strong correlation between conditions that inhibit Ca-ATPase activity and those that promote protein association (Birmachu & Thomas, 1990). In addition, ST-EPR studies of Ca-ATPase rotational dynamics show that enzyme activity correlates with protein rotational mobility (Squier & Thomas, 1988; Squier et al., 1988a,b). Perturbations that increased protein–protein interactions directly through cross-linking decreased ATPase activity, whereas those perturbations that decreased protein–protein interactions increased ATPase activity.

Bee venom melittin is a basic 26 amino acid residue peptide that is a potent agent of cell lysis. The X-ray crystal structure of melittin is known (Terwilliger et al., 1982). Melittin monomers in a hydrophobic environment and melittin tetramers have been shown to assume an amphipathic α-helical structure (Weaver et al., 1989a,b). Melittin binding has been shown to induce various perturbations in membranes, including fusion of lipid vesicles (Morgan et al., 1983), formation of pores in membranes (Hanke et al., 1983), changes in lipid phase (Batenburg et al., 1987; Bradrick et al., 1987), and cell lysis (Dufourc et al., 1986; Tosteson et al., 1985), as reviewed by Dempsey (1990). Melittin is also known to interact with several proteins, including calmodulin (Kataoka et al., 1989; Malencik & Anderson, 1985), protein kinase C (O'Brian & Ward, 1989), myosin light chain (Malencik & Anderson, 1988), and the gastric (H^+/K^+)-ATPase (Cuppoletti et al., 1989; Cuppoletti, 1990).

The interaction of melittin with membranes is of particular interest because of the complex equilibria predicted for the distribution of the amphipathic peptide between the aqueous phase, the membrane surface and proteins, and the hydrophobic core of the membrane. A useful technique in monitoring melittin–membrane interactions is time-resolved spectroscopic measurement of protein rotational diffusion in the bilayer. Previous studies of the effect of melittin on the rotational diffusion of bacteriorhodopsin in reconstituted DMPC vesicles, and band 3 protein in erythrocyte membranes (Hu et al., 1985; Dufton et al., 1984a,b; Clague & Cherry, 1988, 1989), show that melittin can strongly restrict protein rotational diffusion. These studies correlated the aggregation state of the protein with functional changes such as red blood cell hemolysis and mast cell degranulation (Dufton et al., 1984a,b). Other cationic agents such as polylysine and Zn^{2+} were less potent than the amphipathic melittin in aggregating membrane proteins, especially in high-ionic-strength media, indicating that hydrophobic interactions were important in melittin-induced protein–protein interactions (Clague & Cherry, 1989).

In the present study we have used the melittin–SR interaction as a model for further investigation of the relationship between the quaternary structure of the Ca-ATPase and its

† This work was supported by grants from the National Institutes of Health (GM27906 and RR01439). D.M.H. was supported by a predoctoral fellowship from the National Science Foundation.
* To whom correspondence should be addressed.

0006-2960/91/0430-7498$02.50/0

activity. We have measured protein dynamics using time-resolved phosphorescence anisotropy (TPA) and lipid chain dynamics using fluorescence anisotropy of DPH in SR vesicles and correlated these physical parameters with Ca-ATPase activity. The results, in conjunction with analogous EPR studies (Mahaney & Thomas, 1991), provide new insight into the physical basis of Ca-ATPase activity and into the role that amphipathic peptides may play in the regulation of membrane function.

Materials and Methods

Reagents and Solutions. 1,6-Diphenyl-1,3,5-hexatriene (DPH), 1-[4-(trimethyhlammonium)phenyl]-1,3,5-hexatriene, *p*-toluene sulfonate (TMA-DPH), and erythrosin-5-isothiocyanate (ERITC) were obtained from Molecular Probes, Inc. (Eugene, OR) and stored in DMF at −70 °C. ATP, bee venom melittin (approx. 85% pure), catalase, glucose, glucose oxidase type IX, and poly(L-lysine) (MW 3200–3800) were obtained from Sigma. All assays and spectroscopy experiments were carried out at 25 °C in a buffer containing either 60 mM KCl, 6 mM $MgCl_2$, 0.1 mM $CaCl_2$, and 20 mM MOPS, pH 7.0 (denoted as normal ionic strength), or the same buffer plus 0.5 M LiCl (denoted as high ionic strength), unless otherwise stated.

Preparations and Assays. Sarcoplasmic reticulum (SR) vesicles were prepared from rabbit skeletal white muscle and partially purified on a discontinuous sucrose gradient as described previously (Birmachu et al., 1989). These vesicles were suspended in 0.3 M sucrose, and 30 mM MOPS, pH 7.0, and stored in liquid nitrogen. SR protein concentrations were determined by the Biuret method using bovine serum albumin (BSA) as a standard (Lewis & Thomas, 1986). SR purity was checked by using SDS–PAGE as described previously (Birmachu & Thomas, 1990). Ca-ATPase activity was measured in a solution containing either normal or high ionic strength buffer, plus 5 mM ATP, 2 μM of the ionophore A23187, and 0.15 mg of SR protein/mL, essentially as described previously (Lewis & Thomas, 1986).

Melittin was purified by HPLC in the presence of 4 M urea, as described by Wille (1989), with the following modifications: a preparative cation-exchange column (Bio-Rad MA7S, 100 mm × 19 mm) was used at a flow rate of 3.5 mL/min, with the initial isocratic step for the cation-exchange separation changed to %B = 15; the melittin-containing fractions were then loaded onto a preparative Bio-Rad Hi-Pore RP-318 250 mm × 10 mm reverse-phase column, washed, and run over a 0–100% acetonitrile gradient in 0.1% TFA at 2 mL/min for 40 min. We found that this step added a second dimension of purification in addition to desalting the melittin fraction. The purified fractions from the reverse-phase column were lyophilized and stored at −20 °C.

The fraction of melittin bound to SR vesicles was measured by centrifugation. SR, at 0.2 mg of protein/mL, was incubated with melittin for 30 min and then centrifuged at $3.6 \times 10^5 \times g$ for 30 min to pellet the SR–melittin complex. The supernatant was collected, and the fluorescence of melittin's tryptophan residue was used to quantitate the amount of melittin free in solution. The sample was excited with 280-nm light, and the integrated area of fluorescence emission between 325 and 400 nm was measured (with a SPEX Fluorolog II spectrofluorometer) and compared with a standard curve corresponding to known melittin concentrations. The melittin concentration of the supernatant was then subtracted from the total melittin concentration added to determine the concentration of melittin bound to the SR vesicles.

Optical Spectroscopy. The spectrometer used to obtain time-resolved phosphorescence anisotropy (TPA) decays was described previously (Ludescher & Thomas, 1988). The phosphorescence anisotropy decay $r(t)$ is given by

$$r(t) = \frac{I(t)_{vv} - GI(t)_{vh}}{I(t)_{vv} + G2I(t)_{vh}} \quad (1)$$

where $I(t)_{vv}$ and $I(t)_{vh}$ are the time-dependent decays of the phosphorescence intensities observed through polarizers oriented parallel and perpendicular to the vertically polarized excitation pulse. G is an instrumental correction factor. TPA decays of ERITC-labeled Ca-ATPase were collected for 2000 laser pulses, alternating in the vertical and horizontal directions for 30 loops.

Scheme I

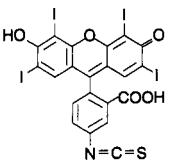

ERITC

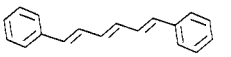

DPH

Time-resolved fluorescence anisotropy (TFA) decays of DPH-labeled SR vesicles were measured by the time-correlated single-photon-counting method (Ware, 1971) on an instrument previously described (Birmachu et al., 1989). TFA anisotropy decays were collected for 40 loops consisting of 10 s of data collection for each of the vertical and horizontal emission-polarizer orientations, with the excitation polarizer set in the vertical position. The excitation function used for the deconvolution of the observed fluorescence decay was obtained by scattering light through a 0.1 mg/mL aqueous glycogen solution at 337 nm. DPH-SR samples were excited at 337 nm, and the emission was collected at 430 ± 10 nm through a Corion S10 interference filter.

Steady-state fluorescence anisotropy was measured with a SPEX Fluorolog II spectrofluorometer. DPH-SR samples were excited with vertical light (at 353 nm), and emission (at 430 nm) was collected for five loops of 20 s in each of the parallel and perpendicular polarizer orientations. This data-collection protocol was found to prevent significant probe bleaching, minimize the effects of time-dependent excitation light fluctuations, and provide data with a good signal-to-noise ratio.

Labeling and Sample Preparation. For phosphorescence experiments, the Ca-ATPase in SR vesicles was specifically labeled on lysine 515 with ERITC as described previously (Birmachu & Thomas, 1990). Oxygen was enzymatically removed from the TPA samples with 100 μg/mL glucose oxidase, 15 μg/mL catalase, and 5 mg/mL glucose, according to the method of Eads et al. (1984). Deoxygenation was carried out in a sealed cuvette (0.3 × 1.0 cm) containing 0.2–0.4 mg/mL SR protein for 10–15 min prior to phosphorescence data collection. For fluorescence measurements of lipid chain dynamics, SR vesicles (0.5 mg/mL) were labeled with DPH or TMA-DPH (added from a 10 mM stock solution in dimethylformamide) at a ratio of 1 mol of DPH per 300 mol of lipid, with an incubation at 4 °C for 1 h in the dark. The samples contained 0.1 mg of protein per milliliter during fluorescence measurements. Samples containing melittin were prepared by adding melittin to the labeled SR and then incubating them for 30 min prior to the acquisition of spectroscopic or enzymatic data.

Data Analysis. Time-resolved phosphorescence anisotropy (TPA) decays were analyzed as reported previously (Birmachu

& Thomas, 1990), by using a nonlinear least-squares fit to a sum of exponentials. Anisotropy decays were fit to a sum of n exponentials plus a constant:

$$r(t)/r_0 = \sum_{i=1}^{n} A_i \exp(-t/\phi_i) + A_\infty \quad (2)$$

where ϕ_i are rotational correlation times, A_i are the normalized amplitudes (r_i/r_0), A_∞ is the normalized residual anisotropy (r_∞/r_0), and r_0 is the initial anisotropy [$r(0) = r_0 = \sum r_i + r_\infty$]. The goodness-of-fit for the anisotropy decays was evaluated by comparing χ^2 values for the multiexponential fits and by comparing plots of the residuals (the difference between the measured and the calculated values).

Time-resolved fluorescence anisotropy (TFA) decays were analyzed by a nonlinear least-squares iterative fitting procedure using the Marquardt algorithm (Hudson et al., 1986). The vertical and horizontal fluorescence decay curves were fit simultaneously to multiexponential functions (convoluted with the excitation light pulse) in order to solve for the lifetime and anisotropy parameters. The computer program for the analysis was provided by Suzanne Hudson and adapted by Franz Nisswandt in our laboratory.

For both TPA and TFA, a model-independent calculation yields $A_\infty = r_\infty/r_0 = S^2$, where S is the order parameter of the probe's transition moment relative to the membrane normal, as affected by rotational motions in the observed time window (Lipari & Szabo, 1980). The rotational motion of membrane proteins or lipids is usually described by one of two models: (a) uniaxial rotation or (b) wobble in a cone [Cherry, 1978; Kawato & Kinosita, 1981; Kinosita & Ikegami, 1984; reviewed by Thomas (1986)]. It has been shown previously (Birmachu & Thomas, 1990) that the TPA of ERITC-SR is dominated by the uniaxial rotation of the labeled Ca-ATPase about an axis normal to the bilayer, with a diffusion coefficient D_m:

$$r(t)/r_0 = A_\alpha \exp(-4D_m t) + A_\beta \exp(-D_m t) + A_\infty \quad (3)$$

Thus each independently rotating species should give rise to two correlation times, $\phi_\alpha = 1/(4D_m)$ and $\phi_\beta = 1/(D_m)$, but it has been shwon that only one of the two decay terms (α or β) is necessary to describe the decay for each rotating species in ERITC-SR (Birmachu & Thomas, 1990). A_∞ describes the extent to which the probe's motion is restricted in angular amplitude, due to the fixed angle Θ_m between the probe's emission transition moment and the membrane normal:

$$A_\infty = S^2 = 1/4(3\cos^2\Theta_m - 1)^2 \quad (4)$$

The rotational diffusion coefficient (D_m in eq 3) for uniaxial rotation of a cylindrical membrane protein can be expressed as a function of the membrane lipid viscosity (η), temperature (T), and the effective radius (a) of the portion of the protein in the bilayer (Saffman & Delbrück, 1975):

$$D_m = kT/(4\pi a^2 h\eta) = 1/(4\phi_\alpha) = 1/\phi_\beta \quad (5)$$

where h is the thickness of the hydrocarbon phase of the lipid bilayer. Thus the rotational mobility ($1/\phi$, which = D_m or $4D_m$ for ERITC-SR) should be proportional to the lipid fluidity [T/η; Squier et al. (1988b)] and inversely proportional to the intramembrane area (πa^2) of the rotating protein. This theory relating protein size and lipid fluidity to protein rotational mobility is supported by previous studies on the Ca-ATPase, as measured by either ST-EPR (Squier et al., 1988a,b) or phosphorescence anisotropy (Birmachu & Thomas, 1990). Therefore, the effective radius a of the Ca-ATPase can be determined from the phosphorescence data if the lipid viscosity

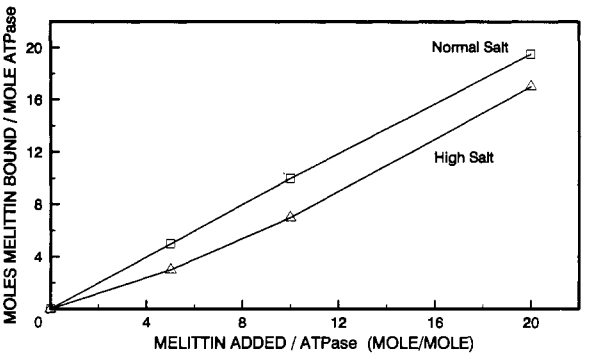

FIGURE 1: Binding of melittin to SR vesicles at normal (60 mM KCl) and high (500 mM LiCl) ionic strength. Binding was measured as tryptophan fluorescence remaining in the supernatant of a centrifuged melittin–SR sample as described under Materials and Methods. Standard deviations were less than 0.5 melittin molecules bound per ATPase molecule.

η is known. Assuming that the other variables remain constant, perturbations in the effective radius of the rotating species can be analyzed by monitoring the amplitudes of the rotational correlation times (A_i), which are indicative of the distribution of a^2 values in the sample and hence to the protein volumes and molecular weights.

It has been shown previously that the TFA of DPH, in SR and other membranes, is best interpreted according to the wobble-in-cone model (Kinosita et al., 1977, 1981; Lipari & Szabo, 1980):

$$A_\infty = S^2 = [\tfrac{1}{2}\cos\Theta_c(1 + \cos\Theta_c)]^2 \quad (6)$$

where Θ_c is the half-angle of a cone, centered on the membrane normal, within which the DPH transition moment wobbles within the experimental time window (0.03–25 ns).

Results

Melittin Binding to SR Membranes. We measured the binding of melittin to SR membranes using the centrifugation protocol described under Materials and Methods. At normal ionic strength, at least 95% of the added melittin was bound to the membranes (Figure 1). The binding of melittin did not saturate. High ionic strength slightly decreased the amount of melittin bound (Figure 1), and these results were used to express the data below in terms of bound melittin.

Melittin Inhibition of SR Ca-ATPase Activity. At normal ionic strength, melittin strongly inhibits the Ca-ATPase activity, with 50% inhibition at 9 ± 1 mol of melittin bound per mole of ATPase (Figure 2). The inhibition of enzymatic activity is biphasic, with a more dramatic effect at low levels of melittin bound. In order to characterize the role of electrostatic interactions on the ATPase activity, we measured enzymatic activity at high ionic strength. The addition of 500 mM LiCl has no significant effect on the first phase of inhibition (bound melittin/ATPase ≤ 3), but it effectively abolishes the second phase of inhibition (Figure 2). Essentially the same results were obtained by using KCl instead of LiCl. Experiments at ionic strengths higher than 500 mM were not attempted, because the ATPase activity in the absence of melittin becomes too low for inhibition studies and previous studies have shown that ionic strengths approaching 1 M convert melittin into its tetrameric form (Quay & Condie, 1983).

Effects of Melittin on Ca-ATPase Rotational Dynamics, Measured by Phosphorescence Anisotropy. The TPA decays of ERITC-labeled Ca-ATPase at various levels of melittin are shown in Figure 3A. Melittin increases the anisotropy, im-

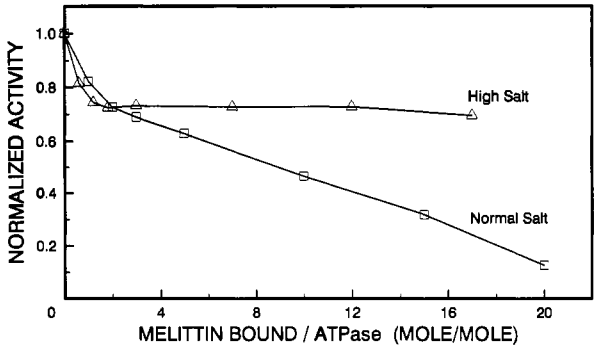

FIGURE 2: Effect of melittin on Ca-ATPase activity at normal and high ionic strength. The activity was divided by the control value in the absence of melittin, then averaged. The eight data points on each curve, from left to right, represent samples containing 0, 1, 2, 3, 5, 10, 15, and 20 mol of melittin *added* per mole of ATPase, respectively. Each point represents at least four data sets, and standard deviations ranged from 0.004 to 0.052. The control values for melittin at normal and high ionic strength were 3.48 IU and 2.37 IU, respectively. Conditions for assays are given under Materials and Methods.

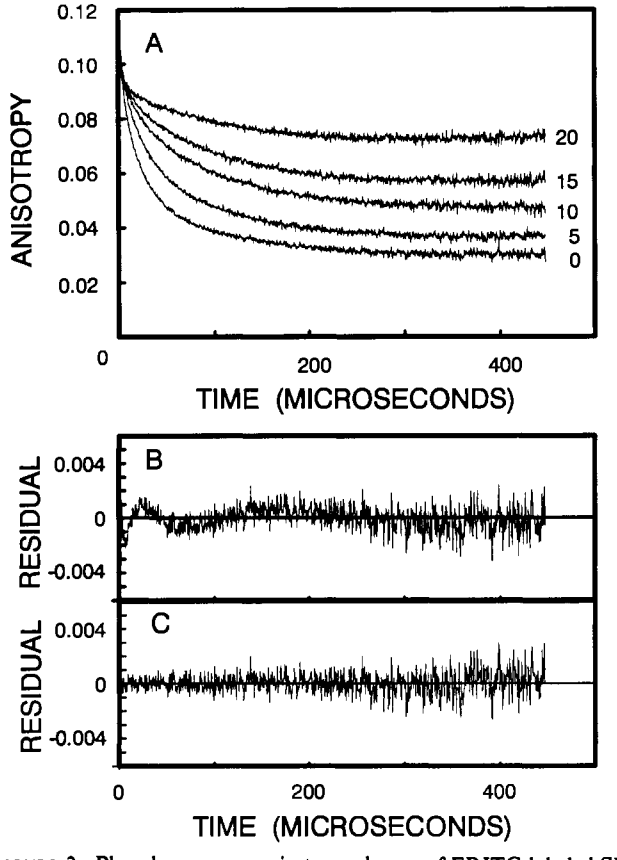

FIGURE 3: Phosphorescence anisotropy decays of ERITC-labeled SR in normal ionic strength buffer at various melittin levels (A). The plot of the residual to the fit of the no-melittin curve using a two-exponential function ($\chi^2 = 2.3$) is shown in panel B. The plot of the residual to the fit of the no-melittin curve with a three-exponential function ($\chi^2 = 1.28$) is shown in panel C. Values displayed at right edge of decays represent the mole ratios of melittin bound per ATPase. Conditions were as given under Materials and Methods for normal ionic strength.

plying decreased microsecond rotational motion. In order to quantitate these effects further, the decays were fit to eq 2. As reported previously (Birmachu & Thomas, 1990), the TPA decays of ERITC-SR are best fit by setting $n = 3$ in eq 2, as judged by the minimization of χ^2 and the randomization of residuals (Figure 3B,C). This was found to be the case in both the presence and absence of melittin. The anisotropy parameters calculated from the three-exponential fits, at the various

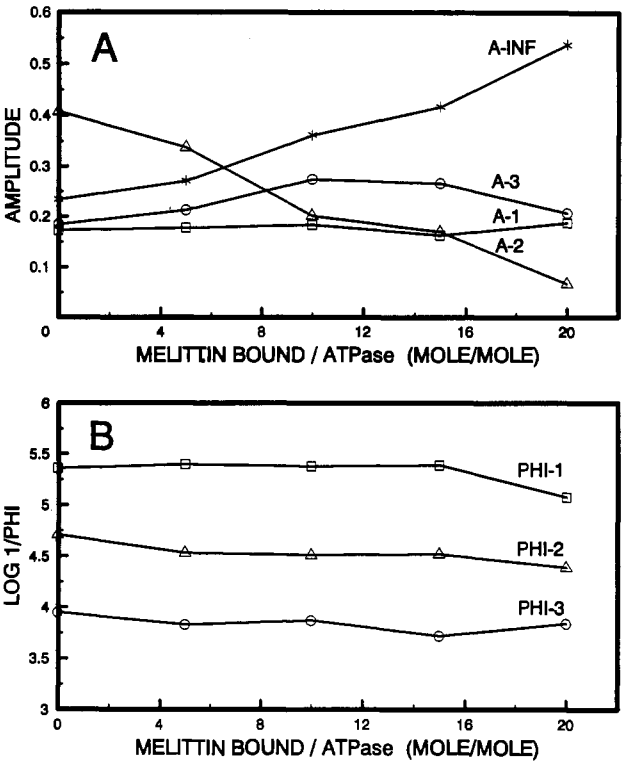

FIGURE 4: Effect of melittin on the phosphorescence anisotropy amplitudes (A) and correlation times (s) (B) from a three-exponential fit of data like that in Figure 3A. Values are averaged over three experiments (see Table I).

concentrations of melittin, are listed in Table I and plotted in Figures 4A and 4B.

The effects of melittin are mainly on the amplitudes A_i (Figure 4A), not the correlation times ϕ_i (Figure 4B) of the TPA decays. The most dramatic effects of melittin are a decrease in A_2, which is proportional to the mole fraction of Ca-ATPase molecules rotating with correlation time ϕ_2 (20–30 μs), and a complementary increase in the residual anisotropy (A_∞), consistent with the conversion of mobile proteins to immobile (presumably aggregated) proteins (Birmachu et al., 1990). The effect of melittin on A_3, which corresponds to the more slowly rotating protein species (ϕ_3 = 100–200 μs), is biphasic, with an initial increase in A_3 that maximizes at approximately 10 melittin/ATPase, followed by a decrease at higher melittin levels. These changes are clearly consistent with a model in which melittin converts mobile species (corresponding to A_2) to less mobile species (corresponding to A_3) and finally to immobile species (corresponding to A_∞). Neither the amplitude (A_1) nor the correlation time (ϕ_1) of the fastest detected rotation is affected by melittin, suggesting an independent mode of motion (e.g., segmental motion within the protein). Molecular models will be analyzed in more detail under Discussion. Above a ratio of 20 melittin/ATPase, the 3-exponential fit of the decay becomes poor due to the vanishingly small values of A_2 and A_3.

Effects of Melittin on TPA at High Ionic Strength. In the high-ionic-strength buffer, melittin had a smaller effect on the phosphorescence anisotropy decay (Figure 5). The principal difference was observed in the residual anisotropy, A_∞ (Figure 5 and Table I). Melittin had no effect on A_∞ up to a melittin/ATPase ratio of 12, despite a substantial increase in A_∞ at normal ionic strength. Above a melittin/ATPase ratio of 12, A_∞ increased to a lesser extent than at normal ionic strength (Figure 2, Table I). Thus, high ionic strength partially inhibits the formation of immobile (presumably aggregated) Ca-ATPase species.

Table I: Phosphorescence Anisotropy Decay Parameters of ERITC-SR[a]

melittin / ATPase	ϕ_1 (μs)	ϕ_2 (μs)	ϕ_3 (μs)	A_1	A_2	A_3	A_∞	r_0	$\langle\tau\rangle$ (μs)
				Normal Ionic Strength (60 mM KCl)					
0	4.4	20	112	0.173	0.408	0.185	0.234	0.114	127
	(2.4)	(2.4)	(19)	(0.053)	(0.054)	(0.027)	(0.017)	(0.009)	(6.2)
5	4.0	29	149	0.178	0.338	0.213	0.271	0.117	110
	(2.4)	(7)	(44)	(0.028)	(0.062)	(0.055)	(0.037)	(0.001)	(3.8)
10	4.2	31	134	0.184	0.202	0.274	0.362	0.115	94
	(3.3)	(11)	(28)	(0.045)	(0.067)	(0.053)	(0.029)	(0.004)	(0.8)
15	4.1	30	192	0.163	0.170	0.266	0.417	0.114	88
	(3.7)	(20)	(101)	(0.063)	(0.093)	(0.028)	(0.053)	(0.006)	(0.4)
20	8.4	40	144	0.188	0.067	0.207	0.538	0.111	87
	(10)	(39)	(41)	(0.037)	(0.027)	(0.021)	(0.074)	(0.005)	(1.0)
				High Ionic Strength (+500 mM LiCl)					
0	4.5	24	204	0.203	0.334	0.232	0.231	0.117	123
	(1.8)	(2.3)	(40)	(0.002)	(0.013)	(0.012)	(0.019)	(0.004)	(12)
3	4.3	38	199	0.202	0.308	0.262	0.228	0.120	97
	(2.5)	(19)	(49)	(0.024)	(0.041)	(0.039)	(0.020)	(0.004)	(4.7)
7	3.7	23	147	0.137	0.263	0.367	0.234	0.118	92
	(2.3)	(4.2)	(30)	(0.086)	(0.094)	(0.063)	(0.021)	(0.011)	(2.9)
12	4.1	33	187	0.202	0.202	0.363	0.233	0.122	94
	(2.7)	(11)	(47)	(0.023)	(0.096)	(0.070)	(0.043)	(0.005)	(3.7)
17	2.9	21	203	0.177	0.086	0.367	0.371	0.120	94
	(1.5)	(10)	(62)	(0.058)	(0.023)	(0.035)	(0.037)	(0.006)	(2.9)

[a] Phosphorescence anisotropy decay parameters obtained from a nonlinear least-squares analysis (parameters defined as in eq 2, with $n = 3$) of phosphorescence anisotropy decays of ERITC-labeled skeletal SR with various amounts of melittin bound per ATPase (mol/mol). Although the same amounts of melittin were added at the two ionic strengths, the bound values were slightly lower at high ionic strength (see Figure 1). $\langle\tau\rangle = \sum a_i\tau_i$ is the average lifetime of the intensity decay fit to

$$I(t) = \sum_{i=1}^{n} a_i \exp(-t/\tau_i)$$

with $n = 4$. Each value in the table is the average from three experiments on separate preparations, with the standard deviation in parentheses.

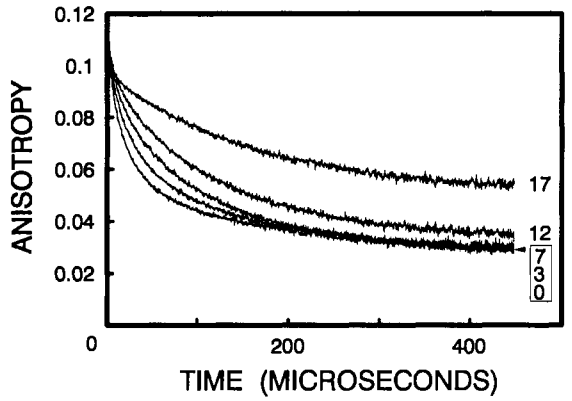

FIGURE 5: Phosphorescence anisotropy decays of ERITC-labeled SR in high-ionic-strength buffer at various melittin levels. Values displayed at right edge of decays represent the mole ratios of melittin bound per ATPase to SR vesicles and correspond to 0, 5, 10, 15, and 20 mol of melittin added per ATPase. Conditions were as given under Materials and Methods for high ionic strength.

Comparison of Polylysine and Melittin. In order to clarify further the role of electrostatics in the melittin–ATPase interaction, we compared the effects of melittin with those of the polycationic peptide polylysine. The two peptides are comparable in size, with an average molecular weight of 3500 and 2840 for polylysine and melittin, respectively. Unlike the amphipathic melittin, polylysine is not expected to interact with the hydrophobic region of the bilayer or with hydrophobic domains in the Ca-ATPase. 2000 times more polylysine than melittin (per ATPase) is required to achieve half-maximal inhibition of Ca-ATPase activity (Figure 6A). The inhibition by polylysine is completely reversed in the high-salt medium, indicating a purely electrostatic interaction of polylysine with the SR membrane. This contrasts with inhibition of the Ca-ATPase by melittin, where 25% of the inhibition is preserved in the presence of 500 mM LiCl, suggesting an additional (presumably hydrophobic) mode of interaction between melittin and SR.

The effects of polylysine and melittin on enzyme function correlate well with their effects on protein mobility, measured by TPA. Addition of 3 mg/mL polylysine to ERITC-SR at normal ionic strength resulted in a substantial restriction of protein mobility, yielding a TPA decay (Figure 6B, top trace) that is comparable to that produced by approximately 10 melittin/ATPase (Figure 3A). However, the restriction of protein mobility by polylysine was completely reversed at high ionic strength (Figure 6B, bottom trace), in contrast to the partial reversal observed with melittin (Figure 5). Thus the correlation between protein mobility and Ca-ATPase activity is very similar when perturbed by polylysine and melittin. Light scattering, presumably due to vesicle aggregation, prohibited the use of higher levels of polylysine in TPA experiments.

Effect of Melittin on Lipid Chain Dynamics, Measured by Fluorescence Anisotropy. In order to quantitate the effects of melittin on lipid hydrocarbon chain dynamics in SR, we measured the time-resolved fluorescence anisotropy of DPH in SR membranes (Figure 7). The intensity (lifetime) and anisotropy (correlation time) parameters were obtained as described under Materials and Methods. Analysis of chi-squared and residual values indicated that two lifetimes and two correlation times were necessary for optimal fits. Table II gives the correlation times and the corresponding amplitudes, along with the model-independent order parameters. Melittin clearly induces a small but significant decrease in DPH rotational mobility, indicated by increases in the principal correlation time and the residual anisotropy. The order parameter increases by 6 ± 2% from 0 to 20 melittin/ATPase. The most variable parameter in the fits was r_0, which limited the precision of the order parameter calculations, especially at high melittin levels. These results are confirmed by the small but

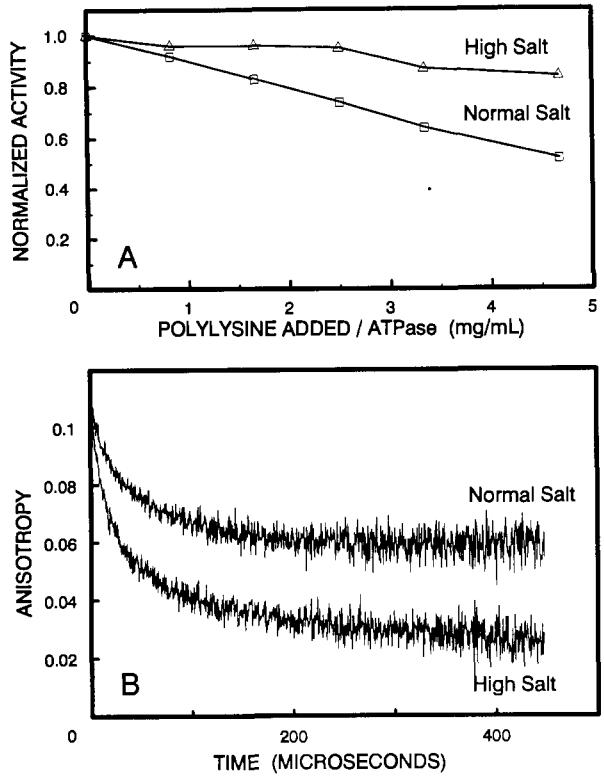

FIGURE 6: (A) Effect of polylysine on Ca-ATPase activity in both the normal and high-ionic-strength buffers. (B) Effect of polylysine on the phosphorescence anisotropy decay of ERITC-labeled Ca-ATPase. Both decay curves contain 3 mg/mL poly(L-lysine). Experiments were performed in either high or normal ionic strength buffer. The decays for both controls (no polylysine, normal ionic strength; no polylysine, high ionic strength) were identical with the lower decay (3 mg/mL polylysine, high ionic strength). Conditions for both sets of experiments are given under Materials and Methods.

significant changes in the steady-state anisotropy (r_{ss} in Table II). The effects of melittin on SR lipid order near the headgroup region were also investigated by using TMA-DPH. Over the range of 0–20 melittin per Ca-ATPase, a similar small change in the steady-state anisotropy was measured with the TMA-DPH probe (not shown). High ionic strength had no significant effects on the melittin-induced steady-state anisotropy increases (data not shown).

Discussion

Summary of Results. Melittin is an effective inhibitor of Ca^{2+}-dependent ATPase activity in SR. TPA of ERITC-labeled SR shows that the addition of melittin also immobilizes the Ca-ATPase in the membrane, as indicated by the increase in both the residual anisotropy and the fraction of rotating species with the longest correlation time. The strong correlation of enzymatic inhibition with protein immobilization, in the absence of comparable effects on lipid fluidity, strongly supports the proposal that Ca-ATPase activity requires microsecond protein rotational mobility and is inhibited by aggregation that reduces this mobility.

Effects on Protein and Lipid Dynamics. The TPA decay of ERITC-SR shows that melittin restricts microsecond rotational motion of the enzyme (Figure 3), changing primarily the pre-exponential factors A_i, without significantly changing correlation times ϕ_i (Table I). It has previously been shown that the TPA decay of ERITC-SR reports primarily the uniaxial diffusion of the Ca-ATPase, i.e., the rotation of the protein about the membrane normal, as predicted by eqs 3–5 (Birmachu & Thomas, 1990). In uniaxial diffusion, each correlation time (ϕ_i) is proportional to the bilayer viscosity (η in eq 5) and to the area of the protein in the membrane plane (πa^2 in eq 5) for a particular rotating species (monomer, dimer, etc.), and each pre-exponential factor (amplitude A_i in eq 2) is proportional to the mole fraction of Ca-ATPase molecules in that species. The nearly invariant correlation times strongly suggest that melittin has little or no effect on the bulk lipid viscosity as defined by eq 5, and this conclusion is supported by the very small effect of melittin on fluorescence anisotropy of the lipid probe DPH.

The most dramatic effect of melittin on the TPA decay (Figures 3 and 4) is a decrease in A_2 (corresponding to $\phi_2 \approx 20$ μs) and a reciprocal increase in the residual anisotropy A_∞, corresponding to an increase in the order parameter S (= $A_\infty^{1/2}$, see Materials and Methods). There are three possible explanations for this: (1) Melittin could decrease the amplitude (cone angle Θ_c) of wobble, for rotation about axes in

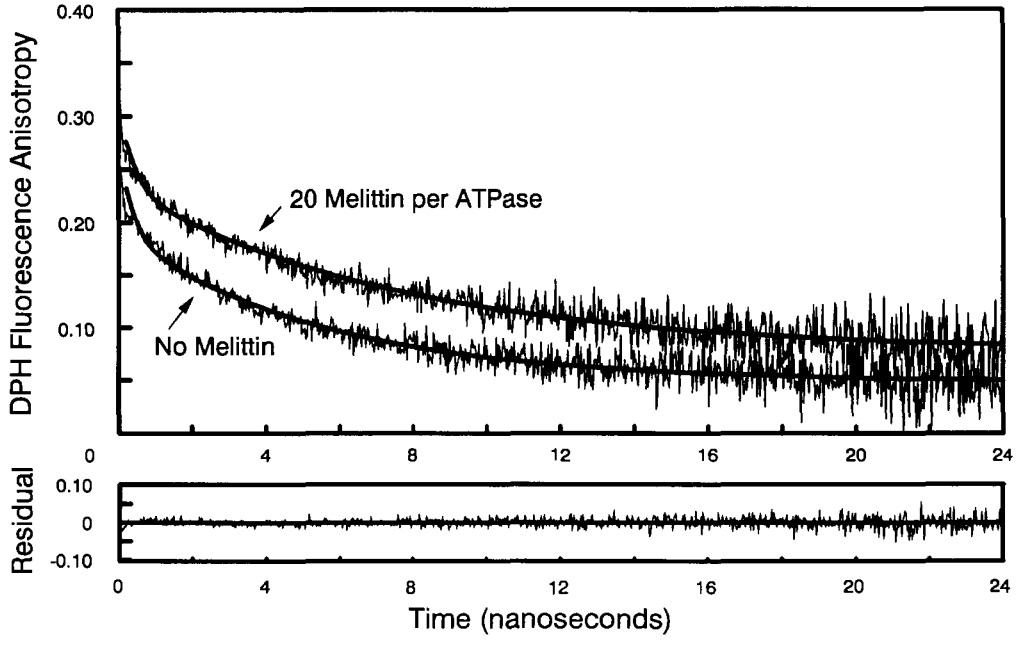

FIGURE 7: Time-resolved fluorescence anisotropy decays of DPH-SR in the absence and presence (20 melittins bound per ATPase) of melittin. The observed decays are superimposed on the fits to two-exponential decays, which have been convoluted with the light pulse (see Table II).

Table II: Time-Resolved and Steady-State DPH Fluorescence Anisotropy Parameters[a]

melittin ATPase	ϕ_1 (ns)	ϕ_2 (ns)	A_1	A_2	A_∞	r_0	S	r_{ss}
0	0.49	5.48	0.36	0.49	0.154	0.321	0.394	0.13
	(0.01)	(0.13)	(0.02)	(0.01)	(0.011)	(0.015)	(0.049)	(0.01)
5								0.14
								(0.01)
10	0.50	6.42	0.30	0.54	0.162	0.321	0.404	0.14
	(0.01)	(0.16)	(0.02)	(0.01)	(0.004)	(0.015)	(0.015)	(0.01)
15								0.15
								(0.01)
20	0.23	7.74	0.42	0.40	0.174	0.385	0.417	0.16
	(0.12)	(0.52)	(0.22)	(0.15)	(0.064)	(0.132)	(0.044)	(0.01)

[a] Melittin/ATPase corresponds to moles of melittin bound per mole of ATPase in SR vesicles. Anisotropy decay parameters (ϕ_i and A_i defined by eq 2) were obtained from two-exponential fits to fluorescence anisotropy and intensity decays, for DPH in SR vesicles. Values of ϕ_i and A_i are the averages from two separate samples. S is the order parameter calculated from $(A_\infty)^{1/2}$. Values in parentheses represent the range of the two averaged time-resolved parameters. r_{ss} is the steady-state anisotropy of DPH in SR, obtained from the average of at least four separately prepared samples, with the standard deviation in parentheses.

the membrane plane (eq 6). This is unlikely, on the basis of the conclusion that the rotation in the absence of melittin is dominated by uniaxial diffusion, not wobble (Birmachu & Thomas, 1990). (2) Melittin could induce a conformational change in Θ_m, the angle between the probe's transition moment and the protein's axis of rotation (the membrane normal) in uniaxial diffusion (eq 4). This cannot be ruled out, but it is unlikely, since (a) there is no precedent for this in previous studies of membrane protein rotation (Thomas, 1986), and (b) the change in A_∞ can be explained more simply without invoking this conformational change, as discussed below. (3) The most likely explanation is an increase in the fraction of proteins rotating on a time scale slower than the window of spectroscopic detection (in this case, 1 ms). In principle, this could be due to a large increase in lipid viscosity (η in eq 5) in a discrete domain of the bilayer. However this is not consistent with the very small effects of melittin on DPH anisotropy (Figure 7, Table II). Thus the increase in A_∞ is almost certainly due to a very large increase (by a factor of 10 or more) in the area (πa^2 in eq 5) of the rotating body in the plane of the membrane, i.e., to large-scale lateral aggregation of the protein. Thus, regardless of the more model-dependent discussion that follows, the present study provides strong and unambiguous support for the conclusions that (1) *melittin induces large-scale protein aggregation in SR*, and (2) *large-scale protein aggregation inhibits Ca-ATPase activity* (Lewis & Thomas, 1986; Squier et al., 1988a; Squier & Thomas, 1988).

Molecular Interpretation of Results. The conclusion that melittin's primary effect on SR is to induce protein association is supported by the pattern of changes in the anisotropy amplitudes A_i (Figure 4), which should be proportional to the mole fractions of populations corresponding to different aggregate sizes (Birmachu & Thomas, 1990). The increase in A_∞ is mirrored by a decrease in A_2, strongly suggesting the conversion of a highly mobile species into large aggregates. However, this conversion may not be direct, since these changes are accompanied by an increase in A_3 at low melittin levels and a decrease in A_3 at high melittin levels, which seems most consistent with the conversion of a mobile species (ϕ_2 = 20–30 μs) into a less mobile (larger, more aggregated) species (ϕ_3 = 100–200 μs) and then into an immobile (very aggregated) species. This progressive aggregation model is quite consistent with the interpretations of temperature effects observed by Birmachu and Thomas (1990). Birmachu and Thomas (1990) were not able to unambiguously assign the component corresponding to A_1 (corresponding to the shortest detected correlation time ϕ_1), which they attributed either to a species undergoing very rapid uniaxial rotation or to intraprotein wobble. This point is clarified by the present study, in which melittin addition at constant temperature produces no change in A_1, despite changes in the other A_i. This suggests that A_1 does not correspond to a uniaxially rotating protein species, but rather to a localized motion (probably intraprotein wobble) that is not affected by melittin.

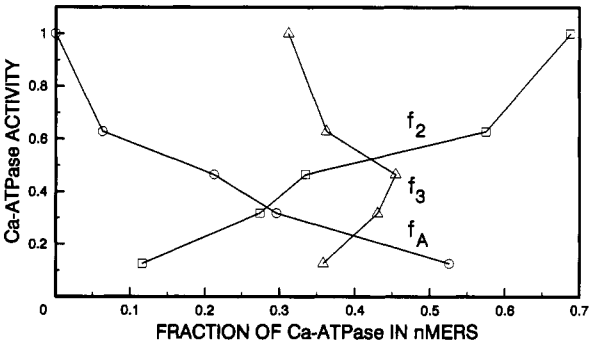

FIGURE 8: Effect of melittin on the distribution of quaternary Ca-ATPase species correlated with enzyme activity. On the basis of model-dependent analysis of the anisotropy amplitudes from Figure 4A (see text), the fractions of Ca-ATPase molecules in the smallest rotating species (f_2), larger oligomers (f_3), and aggregates (f_A) are plotted against Ca-ATPase activity, normalized as in Figure 2. Data are plotted for melittin/ATPase values of 0 (normalized Ca-ATPase activity = 1), 5, 10, 15, and 20.

Thus we associate A_2 with the fastest (smallest) uniaxially rotating protein species, which is aggregated into larger species corresponding to A_3, and ultimately into very large aggregates, which contribute to A_∞. On the basis of this model, the mole fraction f_i of Ca-ATPase molecules in the species corresponding to A_i can be calculated as follows: assuming that there are no large aggregates in the absence of melittin [as concluded by Birmachu et al. (1990)], the mole fraction of Ca-ATPase molecules in large aggregates is $f_A = (A_\infty - A_{\infty 0})/(A_2 + A_3 + A_\infty - A_{\infty 0})$, where $A_{\infty 0}$ is the normalized residual anisotropy in the absence of melittin. The fraction in the smallest species is $f_2 = A_2/(A_2 + A_3 + A_\infty - A_{\infty 0})$, and the fraction of molecules in the intermediate species is $f_3 = A_3/(A_2 + A_3 + A_\infty - A_{\infty 0})$. These fractions and their correlation with Ca-ATPase activity are plotted in Figure 8. This figure clearly shows that enzymatic activity is essentially proportional to f_2, suggesting the most of the activity is in this most mobile population. Similarly, the activity clearly decreases with increasing aggregation (f_A), indicating that the large aggregates are inactive. The correlation with f_3 is not good, suggesting that these intermediate-sized oligomers have intermediate activity.

An unambiguous identification of the specific oligomeric species (corresponding to ϕ_2 = 19.5 μs and ϕ_3 = 112 μs) is not possible, but we can make plausible assignments based on eq 5 (Birmachu et al., 1990). For example, the radius of the intramembrane portion of the Ca-ATPase has been estimated to be 27 Å from X-ray and neutron diffraction data (Herbette et al., 1985) and 20 Å from electron microscopy (Taylor et al., 1986). Substituting these values into eq 5, along with a viscosity of 1.92 poise at 25 °C (Squier et al., 1988b) and a bilayer thickness of 45 Å (Herbette et al., 1985), we obtain predicted rotational correlation times for a Ca-ATPase monomer of 11–19 μs (if $\phi = 1/D_m$) or 3–5 μs (if $\phi = 1/4D_m$). The correlation time for a dimer should be 2–3 times greater than that of a monomer (Jähnig, 1986). Therefore, we conclude that the species corresponding to ϕ_2 (19.5 μs) is a *monomer or a dimer of Ca-ATPase molecules*, and the species corresponding to ϕ_3 (112 μs) is *larger than a dimer*. In fact, it seems likely that the ϕ_3 species is not a well-defined oligomer but could represent a distribution of different oligomers, for which the average size is larger than a dimer.

Electrostatic versus Hydrophobic Effects. The effect of melittin on ATPase activity at normal ionic strength is biphasic (Figure 2), with a steep first phase of inhibition that is unaffected by high ionic strength, suggesting a predominance of hydrophobic interactions, and a more gradual second phase that is reversed by high ionic strength, suggesting a predominance of electrostatic interactions. The effect of high ionic strength on enzyme aggregation (revealed by TPA) is mainly to decrease A_∞. At high ionic strength, melittin appears to convert the monomer/dimer population (A_2) to the intermediate-sized oligomers (A_3), but little is converted into large aggregates (A_∞) (Table I). The cationic peptide polylysine is much less potent than the amphipathic melittin in the inhibition of ATPase activity and in protein aggregation, and polylysine's effects are more completely reversed by high ionic strength. Thus, polylysine's effects appear to be based on purely electrostatic interactions, while melittin's effects are more consistent with this peptide's amphipathic nature. Thus, the melittin–membrane interactions that are responsible for the formation of large aggregates appear to be electrostatic in nature, while the interactions that produce intermediate-sized aggregates (oligomers) appear to be primarily hydrophobic in nature. Further studies will be required to determine which of these electrostatic and hydrophobic interactions involve the lipid phase, the protein, or the protein–lipid interface.

Comparison with EPR Studies. Previous studies in this laboratory have shown that perturbation of the SR by changing temperature (Squier et al., 1988b), selectively cross-linking the enzyme (Squier et al., 1988a), delipidation (Squier & Thomas, 1988), or crystallization of the ATPase using vanadate (Lewis & Thomas, 1986) induces aggregation of the Ca-ATPase within the membrane and results in significant inhibition of enzymatic activity. The observed correlation between ATPase aggregation and enzyme inactivation in these studies suggests that optimal Ca-ATPase mobility facilitates optimal enzyme function. *The present study supports and refines this model, showing that the most active species in the membrane is a monomer or dimer and demonstrating how the mobility and activity of the Ca-ATPase can be regulated by a membrane-active peptide.*

In an EPR study analogous to the present optical study, investigators in this laboratory have studied the effects of melittin on the rotational dynamics of the SR Ca-ATPase (measured by saturation transfer EPR, ST-EPR) and lipids (measured by conventional EPR) (Mahaney & Thomas, 1991). Consistent with the present study, EPR shows that melittin's inhibition of protein rotation is comparable to its inhibition of enzymatic activity but much greater than its effect on lipid fluidity. Beyond these basic results, the EPR and optical data provide complementary information that sharpens our picture of melittin's physical effects on SR. While the time resolution of TFA permits a clear distinction between rate (correlation time) and amplitude (order parameter) effects, only the lipid analogue spin labels provide information about specific depths in the membrane. The EPR results show clearly that melittin's restriction of hydrocarbon chain mobility is significant near the membrane surface but not near the center of the bilayer, indicating that melittin's effects occur mainly at the surface. The detectable effects on lipid spin labels occur mainly at low melittin levels, coinciding with the early phase of ATPase inhibition, which is insensitive to ionic strength. This supports the proposal that this phase of inhibition involves mainly hydrophobic interactions. Another advantage of EPR is that lipid spin labels have been used to develop an empirical measurement of membrane fluidity (T/η; Squier et al., 1988b), which is consistent with the hydrodynamic theory of Saffman and Delbrück (1975) (eq 5). That is, under conditions where lipid dynamics determine protein rotation, the protein's rotational mobility (inverse correlation time) is proportional to T/η, as predicted by eq 5 (Squier et al., 1988b). However, Mahaney and Thomas (1991) showed that the melittin-induced decrease in lipid fluidity (20% near the surface, 5% near the bilayer center) was much less than the decrease in protein mobility (80%), suggesting that protein aggregation, not decreased lipid fluidity, is responsible for melittin's effects. This interpretation was consistent with the ST-EPR measurement of decreased protein mobility (Mahaney & Thomas, 1991), but the time resolution of TPA (present study) was required to show clearly that the melittin affects primarily the amplitudes A_i, not the correlation times ϕ_i (Figure 4B), as predicted for protein aggregation.

Relationship to Other Systems. Previous work by R. Cherry and co-workers on the ability of melittin to immobilize membrane proteins has suggested that a crucial aspect of this action can be attributed to the amphipathic nature of the peptide. By modifying melittin such that its positive charge was reduced by differing degrees, they have shown that the ability of melittin to strongly immobilize band 3 of erythrocyte membranes is dependent on the cluster of positive charges at melittin's C-terminus (Dufton et al., 1984a). In addition, the hydrophobic nature of melittin is also crucial to the peptide's ability to interact with membrane proteins, since melittin's effects on band 3 aggregation are more potent and less ionic-strength-dependent than those of polylysine (Clague & Cherry, 1989). Our results on the Ca-ATPase are consistent with a molecular model proposed by Clague and Cherry (1989) for melittin-induced membrane protein aggregation. In this model the hydrophobic portion of melittin partitions into the bilayer, thereby anchoring the basic moieties close to the membrane surface. The basic groups on the peptide can therefore neutralize repulsion between negative charges on the membrane surface, such as those of phospholipid headgroups and integral proteins. A model consistent with our findings and with those of Clague and Cherry (1989) is illustrated in Figure 9.

Although the addition of melittin to SR is not a direct reconstitution of a physiological event, this analysis of the interactions between one of the best characterized surface-active peptides and one of the best characterized biological membranes should provide insight into a wide range of

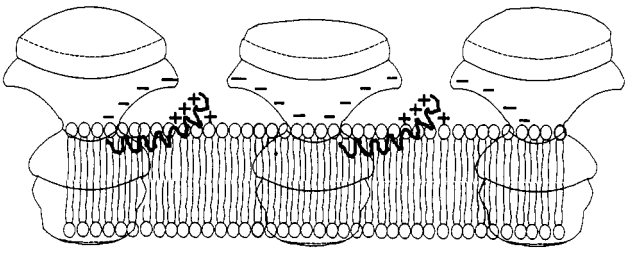

FIGURE 9: Model for melittin-dependent Ca-ATPase aggregation in the bilayer. The hydrophobic portion of melittin is anchored in the membrane with its basic (C-terminal) end exposed, thus screening negative charges on two or more adjacent enzyme monomers or aggregates.

problems in membrane surface biophysics. For example, the present study may be directly applicable to the study of phospholamban, another amphipathic α-helical polypeptide, which plays an important role in the regulation of calcium transport in cardiac SR (Tada & Katz, 1982). More generally, there is a growing roster of basic and/or amphipathic peptides that are known to affect membrane activities, and we hope that some of the lessons learned in the present study will prove applicable to those systems.

ACKNOWLEDGMENTS

We thank Robert Bennett for constructing and maintaining the time-resolved optical spectrometers, and Franz Nisswandt for computer programming. We thank Suzanne Hudson for providing the software used for the TFA fits. We also thank James Mahaney, Derek Marsh, and Frank Prendergast for helpful discussions. Dean Binger, Razvan Cornea, and Amy O'Keefe provided excellent technical assistance.

REFERENCES

Batenburg, A. M., Hibbeln, J. C., Verkeij, A. J., & de Kruijff, B. (1987) *Biochim. Biophys. Acta 903*, 142–154.

Birmachu, W., & Thomas, D. D. (1990) *Biochemistry 29*, 3904–3914.

Birmachu, W., Nisswandt, F. L., & Thomas, D. D. (1989) *Biochemistry 28*, 3940–3947.

Bradrick, T. B., Dasseux, J., Abdalla, M., Aminzadeh, A., & Georghiou, S. (1987) *Biochim. Biophys. Acta 900*, 17–26.

Cherry, R. J. (1978) *Methods Enzymol. 54*, 47–61.

Clague, M. J., & Cherry, R. J. (1988) *Biochem. J. 252*, 791–794.

Clague, M. J., & Cherry, R. J. (1989) *Biochim. Biophys. Acta 980*, 93–99.

Cuppoletti, J. (1990) *Arch. Biochem. Biophys. 278*, 409–415.

Cuppoletti, J., Blumenthal, K. M., & Malinowska, D. H. (1989) *Arch. Biochem. Biophys. 275*, 263–270.

Dempsey, C. E. (1990) *Biochim. Biophys. Acta 1031*, 143–161.

Dufourc, E. J., Smith, I. C., & Dufourcq, J. (1986) *Biochemistry 25*, 6448–6455.

Dufton, M. J., Hider, R. C., & Cherry, R. J. (1984a) *Eur. Biophys. J. 114*, 17–24.

Dufton, M. J., Cherry, R. J., Coleman, J. W., & Stanworth, D. R. (1984b) *Biochem. J. 223*, 1984.

Eads, T. M., Thomas, D. D., & Austin, R. H. (1984) *J. Mol. Biol. 179*, 55–81.

Hanke, W., Methfessel, C., Wilmsen, H., Katz, E., Jung, G., & Boheim, G. (1983) *Biochim. Biophys. Acta 727*, 108–114.

Herbette, L., DeFoord, P., Fleischer, S., Pascolini, D., Scarpa, A., & Blasie, J. K. (1985) *Biochim. Biophys. Acta 817*, 103–122.

Hu, K., Dufton, M. J., Morrison, I., & Cherry, R. J. (1985) *Biochim. Biophys. Acta 816*, 358–364.

Hudson, B. S., Harris, D. L., Ludescher, R. D., Ruggiero, A., Cooney-Freed, A., & Cavalier, S. A. (1986) *Applications of Flourescence in the Biomedical Sciences*, pp 159–202, Alan R. Liss, Inc., New York.

Jähnig, F. (1986) *Eur. Biophys. J. 14*, 63–64.

Kataoka, M., Head, J. F., Seaton, B. A., & Engelman, D. M. (1989) *Proc. Natl. Acad. Sci. U.S.A. 86*, 6944–6948.

Kawato, S., & Kinosita, K., Jr. (1981) *Biophys. J. 36*, 277–296.

Kinosita, K., Jr., & Ikegami, A. (1984) *Biochem. Biophys. Res. Commun. 769*, 523–527.

Kinosita, K., Jr., Kawato, S., & Ikegami, A. (1977) *Biophys. J. 20*, 289–305.

Kinosita, K., Jr., Kataoka, R., Kimura, Y., Gotoh, O., & Ikegami, A. (1981) *Biochemistry 20*, 4270–4277.

Lewis, S. M., & Thomas, D. D. (1986) *Biochemistry 25*, 4615–4621.

Lipari, G., & Szabo, A. (1980) *Biophys. J. 30*, 489–506.

Ludescher, R. D., & Thomas, D. D. (1988) *Biochemistry 27*, 3343–3351.

Mahaney, J. E., & Thomas, D. D. (1991) *Biochemistry* (in press).

Malencik, D. A., & Anderson, S. R. (1985) *Biochem. Biophys. Res. Commun. 130*, 22–29.

Malencik, D. A., & Anderson, S. R. (1988) *Biochemistry 27*, 1941–1949.

Morgan, C. G., Williamson, H., Fuller, S., & Hudson, B. (1983) *Biochim. Biophys. Acta 732*, 668–674.

O'Brian, C. A., & Ward, N. E. (1989) *Mol. Pharmacol. 36*, 355–359.

Qauy, S. C., & Condie, C. C. (1983) *Biochemistry 22*, 695–700.

Saffman, P. J., & Delbrück, M. (1975) *Proc. Natl. Acad. Sci. U.S.A. 72*, 3111–3113.

Squier, T. C., & Thomas, D. D. (1988) *J. Biol. Chem. 263*, 9171–9177.

Squier, T. C., Hughes, S. E., & Thomas, D. D. (1988a) *J. Biol. Chem. 263*, 9162–9170.

Squier, T. C., Bigelow, D. J., & Thomas, D. D. (1988b) *J. Biol. Chem. 263*, 9178–9186.

Tada, M., & Katz, A. M. (1982) *Annu. Rev. Physiol. 44*, 401–423.

Taylor, K. A., Ho, M. H., & Martonosi, A. (1986) *Ann. N.Y. Acad. Sci. 483*, 31–43.

Terwilliger, T. C., Weissman, L., & Eisenberg, D. (1982) *Biophys. J. 37*, 353–361.

Thomas, D. D. (1986) in *Techniques for the Analysis of Membrane Proteins* (Ragan, C. I., & Cherry, R. J., Eds.) pp 377–431, Chapman and Hall, London.

Tosteson, M. T., Holmes, S. J., Razin, M., & Tosteson, D. C. (1985) *J. Membr. Biol. 87*, 35–44.

Ware, W. R. (1971) in *Creation and Detection of the Excited States* (Lamela, A. A., Ed.) Vol. 1A, Marcell Dekker, New York.

Weaver, A. J., Kemple, M. D., & Prendergast, F. G. (1989a) *Biochemistry 28*, 8614–8623.

Weaver, A. J., Kemple, M. D., & Prendergast, F. G. (1989b) *Biochemistry 28*, 8624–8639.

Wille, B. (1989) *Anal. Biochem. 178*, 118–120.